Journal of Organometallic Chemistry 984 (2023) 122561

Contents lists available at ScienceDirect

Journal of Organometallic Chemistry

journal homepage: www.elsevier.com/locate/jorganchem

Luminescent "Chugaev-type" cyclometalated iridium(III) complexes synthesized by nucleophilic addition of hydrazine

Chenggang Jiang‡, Louise M. Cañada‡, Ngoc Bao Nguyen, Thomas S. Teets*

University of Houston, Department of Chemistry, 3585 Cullen Blvd., Room 112, Houston, TX USA 77204-5003

ARTICLE INFO

Article history:
Received 23 August 2022
Revised 6 November 2022
Accepted 10 November 2022
Available online 12 November 2022

Keywords:
Cyclometalated iridium
Luminescence
Carbene ligands
Blue phosphorescence
Electrochemical properties

ABSTRACT

In this work, we describe a series of six neutral Chugaev-type chelating dicarbene iridium complexes with different cyclometalating ligands. The effects of different cyclometalating ligands on the emission properties of dicarbene iridium complexes are evaluated. The triazole- and NHC-derived cyclometalating ligands combine with the strong σ–donating Chugaev-type dicarbene ligand, resulting in phosphorescence that is blue-shifted compared to previously described analogues. The complexes are synthesized by the nucleophilic addition of hydrazine to cationic bis-isocyanide iridium complexes, characterized by ^{1}H, ^{13}C{^{1}H}, and ^{19}F NMR spectroscopy as well as high-resolution mass spectrometry. Four of the six molecular structures of the dicarbene complexes were determined by X-ray crystallography. Electrochemical properties of the compounds were evaluated by cyclic voltammetry analysis, which provides evidence that the HOMO and LUMO energies are dependent on the cyclometalating ligands employed. All the Chugaev-type iridium complexes exhibit blue to blue-green phosphorescence in solution at 77 K and all but one in poly(methyl methacrylate) (PMMA) thin films at room temperature. Although the quantum yields for all the complexes are modest, we succeeded in blue-shifting the emission wavelength of these dicarbene-type iridium complexes.

© 2022 Elsevier B.V. All rights reserved.

1. Introduction

Cyclometalated iridium complexes are one of the most successful classes of organometallic compounds in various applications [1–4], especially in organic light-emitting diodes (OLEDs) [5–8]. Due to the large spin-orbit coupling engendered by the heavy iridium center, these compounds generally exhibit high quantum yields for their color-tunable phosphorescence [9,10]. To be a good candidate for a dopant in the emissive layer of an organic light-emitting diode (OLED), the iridium complex should have high photoluminescence quantum yield at ambient temperature and ideally be charge-neutral to facilitate vacuum deposition fabrication methods [11]. Phosphorescence colors for these neutral iridium complexes range from red to blue [12–14], with blue being the most challenging to generate due to its requirement of a high HOMO–LUMO energy gap to achieve high-energy photoluminescence. Due to the large energy gap and destabilization of the LUMO energy, dissociative metal-centered ligand-field states (^{3}MC) become more accessible, which introduces a nonradiative decay pathway that limits the efficiency and stability of blue emitters.

For charge-neutral iridium complexes, there are two major structural classes: homoleptic complexes with the general formula [Ir(C^Y)$_3$] (C^Y = cyclometalating ligand), usually the facial (*fac*) isomer [15,16], and heteroleptic [Ir(C^Y)$_2$(LX)] complexes [17,18], where (LX) is a monoanionic chelating ancillary ligand. To achieve high-energy phosphorescence, the cyclometalating ligands (C^Y) must be carefully selected, since the emission for these iridium complexes is often controlled by the structure of the cyclometalating ligand [19]. A good choice of cyclometalating ligands would be those that destabilize the LUMO and stabilize the HOMO to create a large energy gap. Aryl-triazoles and N-heterocyclic carbenes (NHCs) meet these criteria and have been used in blue-phosphorescent iridium complexes [20–22]. The HOMO of these complexes is associated with the metal center and the aryl ring, while the LUMO is mainly localized on the triazolyl or imidazolyl heterocycle. Electron-withdrawing groups on the aryl ring and electron-donating substituents on the *N*-heterocycle can further increase the HOMO–LUMO gap. In this study, two classes of aryl-triazole-based cyclometalating ligands (with 1,2,3-triazole or 1,2,4-triazole heterocycles) are used along with NHC-based cyclometalating ligands to engender blue phosphorescence.

Aside from the careful design of the C^Y ligand, the selection of an appropriate ancillary ligand is also crucial to fine-tune the photoluminescence properties of heteroleptic iridium complexes [23].

* Corresponding author at: University of Houston, United States.
E-mail address: tteets@uh.edu (T.S. Teets).
‡ Chenggang Jiang and Louise M. Cañada contributed equally.

https://doi.org/10.1016/j.jorganchem.2022.122561
0022-328X/© 2022 Elsevier B.V. All rights reserved.

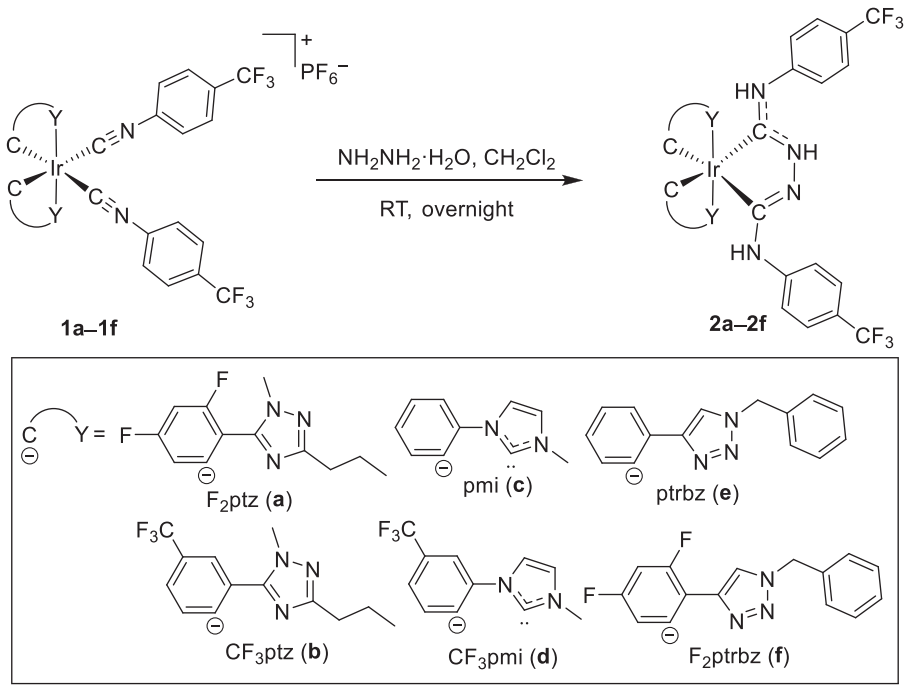

Scheme 1. Synthesis of "Chugaev-type" dicarbene complexes.

In heteroleptic complexes, the ancillary ligand not only can sometimes influence the emission wavelength, but also can have a large impact on redox properties and excited-state dynamics. "Chugaev-type" chelating acyclic diaminocarbenes (ADCs), studied for over 100 years as the oldest carbene ligand class, [24–27] are attractive for blue-phosphorescent iridium complexes because of their strong σ-donating character and high stability. Previously, our group reported a straightforward method to install these dicarbene ligands onto bis-cyclometalated iridium complexes, resulting in good photoluminescence properties, especially for sky-blue emitters immobilized in PMMA film [28,29]. We have also installed other types of monodentate or cyclometalated ADC ligands onto platinum [30,31] or iridium [19, 32] complexes, which are particularly effective for supporting efficient deep-blue phosphorescence.

These previous studies have motivated us to explore Chugaev dicarbenes as supporting ligands for compounds with phosphorescence deeper in the blue region, and those efforts are described here. The compounds in this study feature triazole- and NHC-based cyclometalating ligands known to result in pure blue to deep blue phosphorescence. We introduce a series of six compounds all with different C^Y ligands, produced by the reaction of cationic bis-isocyanide iridium precursors with hydrazine. This efficient ligand-centered functionalization strategy gives access to these complexes in excellent yields. A detailed description of the electrochemical and photophysical properties reveals the electronic influence of the Chugaev carbene on these compounds. Despite the judicious choice of cyclometalating ligands, the compounds all luminesce in a similar sky-blue to blue-green region of the spectrum, which we attribute to a low-lying charge-transfer excited state involving the Chugaev dicarbene.

2. Results and discussion

2.1. Synthesis

Scheme 1 outlines the synthetic method for these carbene complexes, following a procedure previously reported by our group [28]. The six new compounds differ with respect to their cyclometalating ligands (C^Y), which come from the aryl-triazole or aryl-NHC families with structures and abbreviations also summarized in Scheme 1. Preparation of the precursor bis-isocyanide complexes **1a, 1b**, and **1d** has been previously described [33], whereas precursors **1c, 1e**, and **1f** were synthesized following the same route and characterized by ^{1}H and ^{19}F NMR spectroscopy (Fig. S1–S6 of the Supplementary material). The bis-cyclometalated bis-isocyanide iridium complex was dissolved in minimum CH_2Cl_2 and mixed with a large excess of hydrazine monohydrate ($>$ 200 equiv). The reaction mixture was stirred overnight at ambient temperature and atmosphere. Biphasic extraction and recrystallization were sufficient to purify all complexes, which were isolated in good to excellent yields ranging from 56–92%. The identity and purity of the neutral "Chugaev-type" carbene complexes were ascertained through high-resolution ESI-MS, and ^{1}H, ^{19}F, and ^{13}C{^{1}H} NMR spectroscopy (Fig. S7–S20 of the Supplementary material). All experimental values for HRMS-ESI match within $<$ 0.01% error of the theoretical values. ^{1}H NMR spectra of **2a–2f** show two broad N–H signals in a 1:2 ratio. The downfield N–H peak near δ = 10 ppm can be assigned to the backbone N–H, known to be more acidic than the exterior N–H bonds. The other N–H peak in the range of δ 6.65–6.40 ppm corresponds to the exterior N–H protons, which are located outside the chelate ring. The NMR spectra of all six "Chugaev-type" carbene complexes are consistent with C_2 symmetry, which suggests rapid tautomerization of the asymmetric dicarbene backbone in room temperature solutions. The thermal stabilities of complexes **2c** and **2e** were qualitatively evaluated (Fig. S22–S23 of the Supplementary material) as representative examples of this class of iridium complexes. The compounds were dissolved in $CDCl_3$ at millimolar concentrations and initially held at room temperature before heating to 60°C. No decomposition was observed for up to 48 h at room temperature, and only a small amount of degradation was observed after 48–96 h at 60°C, with the majority of the compound remaining intact. As such, we can conclude that these "Chugaev-type" dicarbene iridium complexes are not prone to thermal decomposition.

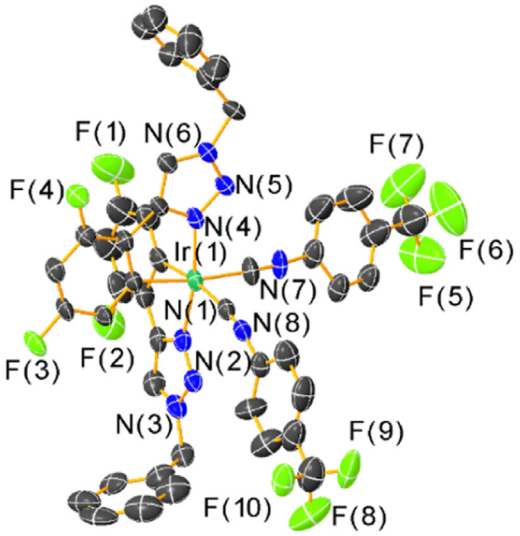

Fig. 1. Molecular structure of **1f**, determined by single-crystal X-ray diffraction. One of the two crystallographically independent molecules is shown. Thermal ellipsoids are shown at the 50% probability level. Hydrogen atoms, counterions, and solvent molecules were omitted for clarity.

2.2. Crystal structures

The molecular structure of one of the new bis-isocyanide precursor complexes, **1f**, was determined by X-ray crystallography and is shown in Fig. 1. Like many other related structures from our group, the two isocyanide ligands are arranged in a *cis* orientation, with nearly linear C≡N–C bond angles that indicate only a small degree of π-backbonding from the iridium(III) center. Refinement data for **1f** is summarized in Table S1 of the Supplementary material.

The molecular structures of four of six "Chugaev-type" dicarbene iridium complexes were confirmed by x-ray crystallography, with three (**2a, 2b**, and **2d**) shown in Fig. 2. The structure of **2c** did not refine as well due to non-merohedral twinning, but the molecular structure was confirmed and is displayed in Fig. S21. The crystallographic data and refinement parameters for these compounds are reported in Tables S1–S3. The coordination geometry around the iridium center in each Chugaev carbene complex is distorted octahedral, completed by two C^Y ligands and one "Chugaev-type" dicarbene ancillary ligand. As is typical in bis-cyclometalated iridium complexes [34,35], the triazole rings in **2b** and imidazole rings in **2d** of the cyclometalating ligands occupy a *trans* arrangement. However, complex **2a** formed a co-crystal where the asymmetric contains two independent molecules: one has the C^Y triazole heterocycles arranged in the usual *trans* disposition (*trans*-**2a**), the other with a *cis* arrangement of the C^Y heterocycles (*cis*-**2a**). We believe that the *cis* isomer either represents a very minor impurity in the crystallized sample or that isomerization occurred during crystallization, as the bulk isolated sample of **2a** shows only a single product in the ^{1}H and ^{19}F NMR spectra, with a pattern of peaks consistent with the approximate C_2 symmetry of the *trans* isomer (Fig. S7 and S8). In the chelating bis-ADC ancillary ligand structure of all complexes, the backbone N–H hydrogen atom is localized in the solid state to afford C_1 molecular symmetry, indicating that unlike in solution at room temperature, the N–H proton does not tautomerize at 123 K in the solid state. Bond distances in the bis-ADC ligands are within 0.02 Å of those structures our group has previously reported [28,29], and bond angles are within 4°. The Ir–$C_{carbene}$ bond lengths range from 1.992(7) Å to 2.066(7) Å. For all three complexes, the dicarbene bite angles (C–Ir–C) span a narrow range of 75.94(10)–76.9(3)°, and the N–$C_{carbene}$–N bond angles range from 116.3(2)° to 118.4(6)° and indicate formal sp^2 hybridization of the carbene carbon atoms.

Table 1
Summary of electrochemical data for complexes **2a**–**2f** and previously reported dicarbene complexes. All potentials are reported relative to Fc^+/Fc and represent peak anodic (E^{ox}) or cathodic (E^{red}) potentials.

	E^{ox} / V	E^{red} / V
$Ir(F_2ppy)_2(C_2H_3N_4(Ar^{4\text{-}CF3})_2)$[a]	0.98, 1.19, 1.46	−2.47, −2.78
$Ir(bt)_2(C_2H_3N_4(Ar^{4\text{-}CF3})_2)$[a]	0.86, 1.02, 1.47	−2.31, −2.45, −2.64
2a	0.33, 1.16, 1.32	−2.74
2b	0.32, 1.10, 1.29	−2.66
2c	0.17, 0.68, 0.84, 1.23	−2.76
2d	0.20, 0.90, 1.06, 1.49	−2.79
2e	0.18, 0.76, 0.95	−2.77
2f	0.20, 0.88, 1.01	−2.85

[a] Chugaev complexes from our previous reports are included for easy comparison[28,29] (F_2ppy = 2-(2,4-difluorophenyl)pyridine and bt = 2-phenylbenzothiazole).

2.3. Electrochemistry

Cyclic voltammograms of complexes **2a**–**2f** are plotted in Fig. 3 and redox potentials are summarized in Table 1, with the corresponding first oxidation peak shown in inset graphs. Similar to previously reported analogous iridium complexes [28,29], all compounds show irreversible redox peaks. Cathodic scans are shown as red traces in Fig. 3 and all complexes show one irreversible reduction peak. For all six complexes, this reduction occurs at −2.66 to −2.85 V, meaning they are much more difficult to reduce compared to their respective bis-isocyanide precursor [33] and that the LUMO is destabilized when two isocyanide ligands are converted into a Chugaev dicarbene ligand. Substituents on the cyclometalating ligand exert subtle effects on the reduction potentials, which should be cautiously interpreted since they are all irreversible waves. When comparing complexes **2a** and **2b**, which both have triazole-based cyclometalating ligands, changing the substituent on the phenyl ring of the ptz ligand to a more electron-withdrawing CF_3 group shifts the reduction peak by 80 mV to a more positive potential (from −2.74 to −2.66 V). However, the opposite trend was observed by comparing the pairs **2c**/**2d** and **2e**/**2f**. In complex **2c**, the reduction potential is −2.76 V, while in complex **2d**, which has an additional electron-withdrawing CF_3 group on each C^Y ligand, the reduction potential shifts negatively to −2.79 V. Similarly, the reduction potential occurs at −2.77 V in complex **2e** and cathodically shifts to −2.85 V in complex **2f**, where there are two fluorine substituents on the phenyl ring of each ptrbz ligand.

The effect of changing the triazole-based cyclometalating ligand to an imidazole-based ligand can be observed by comparing complex **2b**, which has the CF_3ptz ligand, and complex **2d**, which has the CF_3pmi ligand. Both have a CF_3 group para to the C–Ir bond. Replacing the triazole with an imidazolyl moiety cathodically shifts the reduction potential by 130 mV, from −2.66 V in complex **2b** to −2.79 V in complex **2d**. The reduction potential of **2a** (1,2,4-triazole) is −2.74 V, with **2f** (1,2,3-triazole) about 110 mV more negative, suggesting that the triazole isomer present in the C^Y ligand also has a significant effect on the LUMO energy level.

Anodic scans are shown as black traces in Fig. 3 and at least three irreversible oxidation peaks are observed for all complexes. Oxidation peaks for all complexes range from 0.17 to 1.49 V. Previously reported carbene complexes have more positive first oxidation peaks (at least 0.86 V), suggesting that the carbene and triazole complexes **2a**–**2f** are relatively easier to oxidize compared to previous analogues with pyridine or benzothiazole-based C^Y ligands [28,29]. By comparing the first oxidation peak potentials in the pairs **2a**/**2b, 2c**/**2d**, and **2e**/**2f**, there is no significant shift when

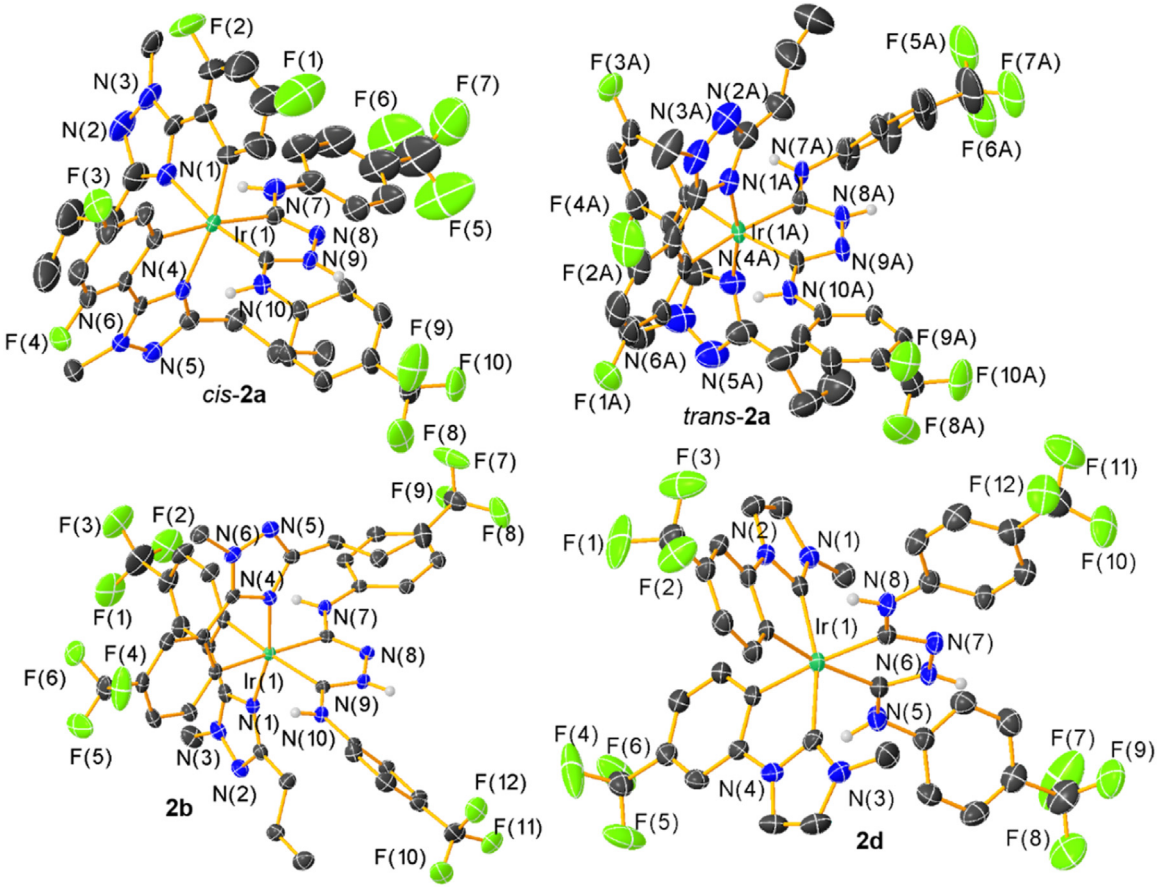

Fig. 2. Molecular structures of **2a**, **2b**, and **2d**, determined by single-crystal X-ray diffraction. Thermal ellipsoids are shown at the 50% probability level. Hydrogen atoms bonded to carbon and solvent molecules were omitted for clarity.

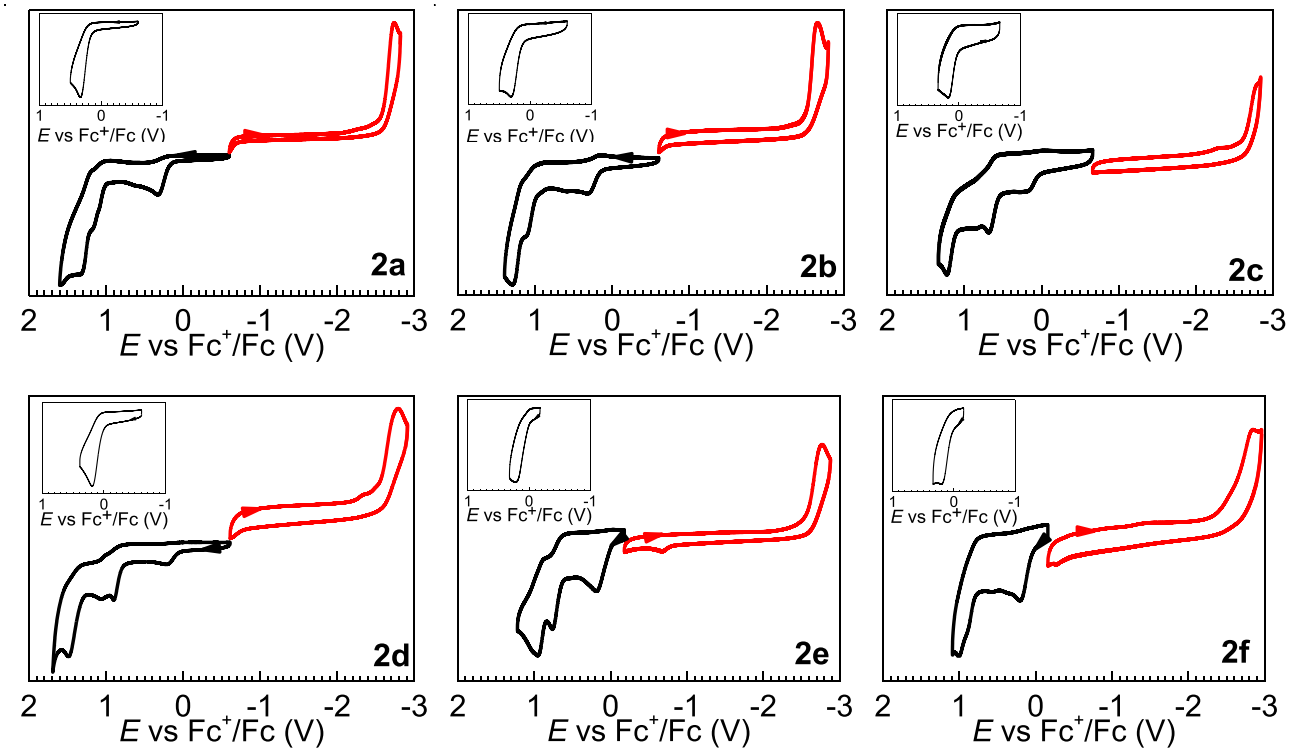

Fig. 3. Cyclic voltammograms of complexes **2a**–**2f**, recorded in acetonitrile with 0.1 M $TBAPF_6$ electrolyte. The arrows indicate the scan direction. Insets show an anodic sweep scanning only past the first oxidation wave, which remains irreversible in each case.

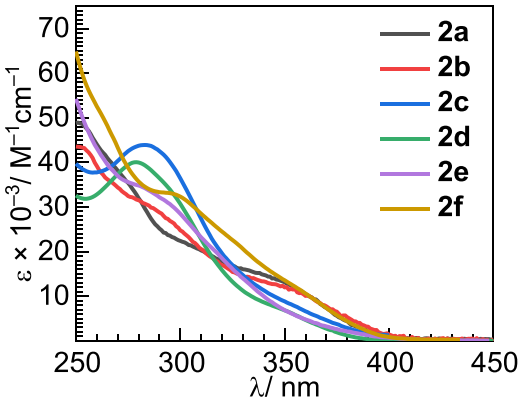

Fig. 4. UV–vis absorption spectra of complexes **2a**–**2f**, recorded in CH_2Cl_2 at room temperature. Spectra were recorded over a range of ca. 10^{-6} to 10^{-5} M, and a Beer's Law plot was used to determine molar absorptivity values.

electron-withdrawing groups have been added to the cyclometalating ligand, which signifies that electron-withdrawing substituents on the aryl ring do not greatly influence the oxidation peak potential and the majority of the HOMO does not lie on this ring. All six complexes have large HOMO–LUMO gaps of at least 3.05 eV, estimated from the separation of the first anodic and first cathodic peaks, a requisite feature for blue phosphorescence.

2.4. Photophysical properties

UV-vis absorption spectra for the complexes **2a**–**2f** were recorded in CH_2Cl_2 solutions at room temperature, shown in Fig. 4. In general, electron-withdrawing groups on the cyclometalating ligands have minimal impacts on the UV-vis absorption, although the profile in fluorinated F_2ptrbz complex **2f** is notably red-shifted from that of the unsubstituted analogue **2e**. Nevertheless, all complexes in this study absorb only in the UV region, with similar molar absorptivity values for the respective bands. The intense bands in the region of 230–320 nm are assigned to spin-allowed π–π^* transitions localized on the cyclometalating and Chugaev dicarbene ligands. All six complexes display weaker, overlapping shoulders tailing off near the start of the visible region (~400 nm), which are attributed to both spin-allowed and spin-forbidden metal-to-ligand charge transfer (MLCT) transitions

Photoluminescence spectra were recorded both in solution and in transparent PMMA films doped with 2 wt% of the respective complex. The data are collected in Fig. 5. These dicarbene complexes do not emit in CH_2Cl_2 solution at room temperature, and complex **2a** also does not exhibit photoluminescence in PMMA thin film at room temperature. Photoluminescence spectra in 2 wt% PMMA thin film at room temperature are shown as blue dashed lines, and in CH_2Cl_2/toluene glass at 77 K as red lines (Fig. 5), with the data summarized in Table 2. The emission wavelengths in **2a, 2b,** and **2d** have a sizable red shift relative to their precursor bis-isocyanide complexes [33]. In addition, less clear vibronic structure is observed in the low-temperature emission spectra of **2a**–**2f** compared to bis-isocyanide complexes [33,35,36], suggesting more charge-transfer character in the excited state of dicarbene complexes. Slight rigidochromic blue shifts were observed for complexes **2c**–**2f** when recorded at 77 K in solvent glass (862 cm^{-1}, 1095 cm^{-1}, 1329 cm^{-1}, and 800 cm^{-1}, respectively), which further evinces significant charge-transfer character in the emissive excited state. Adding electron-withdrawing groups to 1,2,4-triazole-based cyclometalating ligands results in a small blue shift (**2a** vs. **2b**), as expected, corresponding to the larger HOMO−LUMO gap in the CV (Fig. 3). In the pair of **2c**/**2d**, the additional CF_3 group on the pmi ligand does not have a large impact on the emission spectrum, which is consistent with the minimal change in redox potentials caused by this substitution. However, the emission wavelength did not change much in the case of the substituted ptrbz complexes (**2e** and **2f**), despite the fluorinated analogue (**2f**, C^Y = F_2ptrbz)

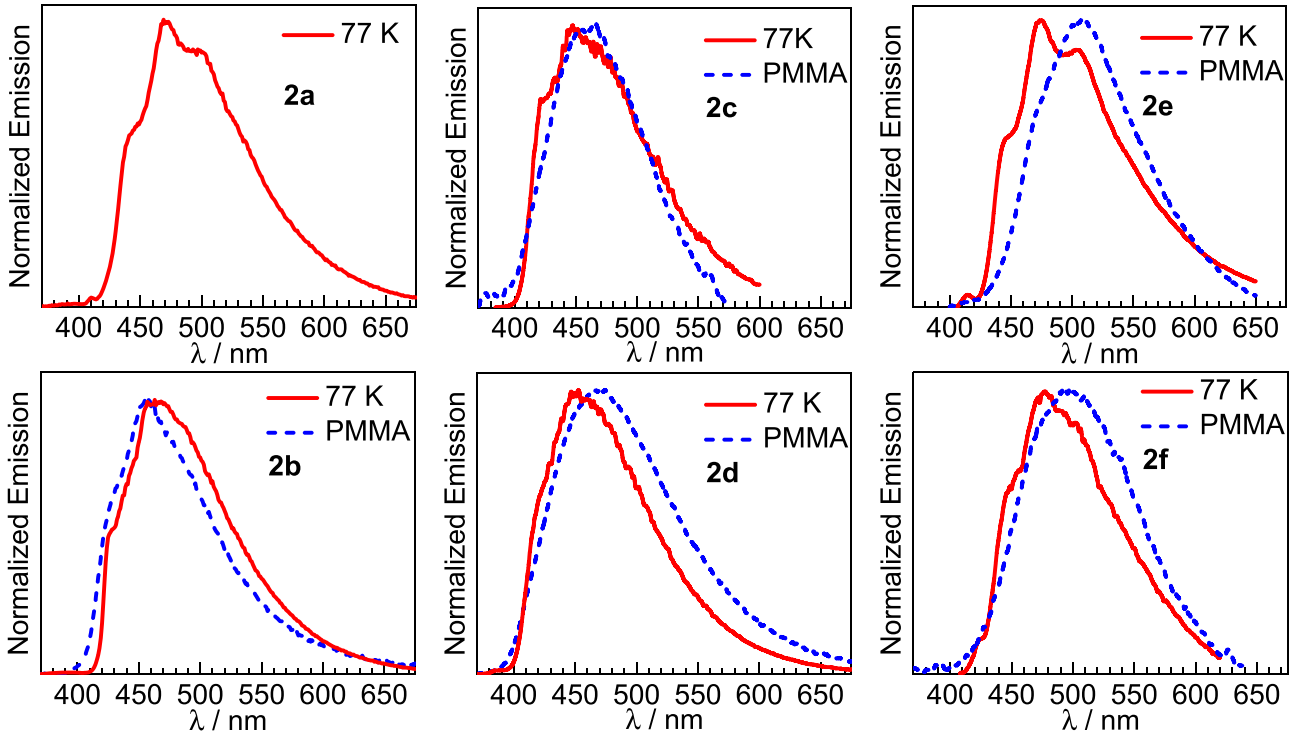

Fig. 5. Overlaid photoluminescence emission spectra of complexes **2a**–**2f**. Photoluminescence spectra are shown in 2 wt% PMMA thin film at room temperature (blue dashed line) and in CH_2Cl_2/toluene glass (ca. 10^{-6} to 10^{-5} M) at 77 K (red solid line).

Table 2
Summary of photophysical data for complexes **2a**–**2f**.

	UV-vis Absorption	Photoluminescence		
	λ / nm	77 K	PMMA, RT	
	($\varepsilon \times 10^{-3}$ / $M^{-1}cm^{-1}$)	λ / nm	λ / nm	Φ_{PL}
2a	276 (35), 350 (13)	440(sh), 469, 500	a	a
2b	285 (30), 355 (12)	427(sh), 463, 488(sh)	428(sh), 457, 490(sh)	0.034
2c	284 (44), 351 (8.6)	422 (sh), 448	466(br)	0.15
2d	279 (40), 352 (6.5)	447	470(br)	0.082
2e	278 (21), 354 (3.7)	415(sh), 445(sh), 475, 503(sh)	469(sh), 507	0.027
2f	297 (33), 359 (11)	423(sh), 448(sh), 478, 507 (sh)	497	0.029

a This compound is not luminescent at room temperature in PMMA thin film.

having a larger electrochemical HOMO−LUMO gap. Acknowledging that the electrochemical gaps may not be truly indicative of HOMO–LUMO separations on account of the irreversible nature of the redox couples, this observation also suggests that the phosphorescent triplet state of these compounds is not a pure HOMO–LUMO transition.

Photoluminescence quantum yields of **2a**−**2f** are modest in PMMA films, significantly lower than the bis-isocyanide precursor complexes where such comparisons are available. [33] Our tentative explanation is that the conjugated dicarbene serves as a chromophore and introduces a new low-lying excited state which is weakly luminescent. As discussed above, the emission spectra of **2a**–**2f** are all very similar to one another, with subtler dependence on the cyclometalating ligands than we would normally expect for this subset of triazole- and NHC-derived C^Y ligands. In most cases, particularly for NHC-based complexes **2c** and **2d**, the spectra are significantly red-shifted from those of other bis-cyclometalated iridium complexes with the same C^Y ligands, [19,33] indicating the Chugaev ligand that is common to **2a**–**2f** could be involved in the luminescent excited state. Whatever the precise origin of these observations, they suggest that Chugaev dicarbenes are not ideally suited to be supporting ligands for deep blue-phosphorescent cyclometalated iridium complexes, since they have the effects of both shifting the luminescence out of the deep blue region and resulting in modest quantum yields.

3. Conclusions

To summarize, six charge-neutral dicarbene-supported cyclometalated iridium complexes were generated by chelative insertion of hydrazine into cis-oriented aryl isocyanides on the cationic precursor complexes. This ligand-centered functionalization produces an acyclic diaminocarbene ancillary ligand, with the target complexes isolated in good yield. Four of these “Chugaev-type” complexes have triazole-based cyclometalating ligands (F_2ptz, CF_3ptz, ptrbz, and F_2ptrbz), and the rest employ imidazolyl-based C^Y ligands (pmi and CF_3pmi). None of the complexes exhibit phosphorescence in solution at room temperature, and all are negligibly to modestly luminescent when immobilized in PMMA films. For complexes that were found to be emissive in PMMA thin film, photoluminescence quantum yields are lower and emission maxima are red-shifted compared to their corresponding bis-isocyanide complexes, albeit in a similar spectral range or slightly blue-shifted relative to other iridium dicarbene complexes our group has reported. This shows that using cyclometalating ligands with a triazole or NHC moiety can blue-shift the photoluminescence relative to pyridyl-based analogues, although not to as large as an extent as is normally possible with these classes of cyclometalating ligands. This work generalizes the synthesis of bis-cyclometalated iridium complexes with Chugaev dicarbenes and shows that the dicarbene has significant effects on the phosphorescence, although not always beneficial. Because of their modular synthesis, stability, and electronic characteristics Chugaev dicarbenes are an intriguing class of supporting ligands for luminescent organometallic complexes, although this work suggests they may not be well-suited for applications in deep-blue phosphorescence.

4. Experimental section

4.1. Materials

Reactions were performed in ambient conditions. Solvents for photophysical measurements and electrochemical measurements were obtained from a Grubbs Solvent Purification System and degassed with argon. Commercially available starting materials and reagents were used without further purification. Tetrabutylammonium hexafluorophosphate, used as a supporting electrolyte for cyclic voltammetry experiments, was recrystallized from hot ethanol, and ferrocene, used as an internal standard for cyclic voltammetry experiments, was purified by sublimation. The iridium dimers of the general formula $[Ir(C^Y)_2(\mu\text{-}Cl)]_2$ (C^Y = cyclometalating ligand) were prepared by following literature procedures. [37] The precursors $[Ir(C^Y)_2(CNAr^{4\text{-}CF3})_2][PF_6]$, where C^Y = F_2ptz (**1a**), CF_3ptz (**1b**), or CF_3pmi (**1d**) and $CNAr^{4\text{-}CF3}$ = 4-trifluoromethylphenyl isocyanide, were synthesized according to our previous report [33]. The other three $[Ir(C^Y)_2(CNAr^{4\text{-}CF3})_2][PF_6]$ precursors were prepared using an identical synthetic procedure, which is detailed below.

4.2. Physical methods

^1H, ^{19}F and $^{13}C\{^1H\}$ NMR spectra were recorded at room temperature using a JEOL ECA-400, ECA-500, or ECA-600 NMR spectrometer. The ESI-MS experiments were carried out at The University of Texas at Austin’s Mass Spectrometry Facility using an Agilent 6530 Q-TOF mass spectrometer and operated in positive ionization mode, with a capillary voltage of 3.5 kV. UV−vis absorption spectra were measured in dichloromethane solutions in 1 cm quartz cuvettes sealed with a screw cap and septum, using an Agilent Cary 8454 UV−vis spectrophotometer. Steady-state emission spectra were measured using a Horiba FluoroMax-4 spectrofluorometer with appropriate long-pass filters to exclude stray excitation light from detection. To exclude air, samples for emission spectra were prepared in a nitrogen-filled glovebox using dry, deoxygenated solvents, and thin-film PMMA samples were kept under nitrogen until immediately before measurement. Samples for low-temperature emission were contained in a quartz EPR tube with a high-vacuum valve and cooled in liquid nitrogen using a finger Dewar. The absolute quantum yields of complexes doped into poly(methyl methacrylate) (PMMA) thin films were recorded using a Spectralon-coated integrating sphere integrated with a Horiba FluoroMax-4 spectrofluorometer. Cyclic voltammetry (CV) measurements were performed with a CH Instruments 602E potentiostat using a three-electrode system in a nitrogen-filled glovebox.

A 3 mm diameter glassy-carbon electrode, Pt wire, and silver wire were used as working electrode, counter electrode, and pseudoreference electrode, respectively. Measurements were carried out in acetonitrile solution with 0.1 M $TBAPF_6$ as a supporting electrolyte at a scan rate of 0.1 V/s. Ferrocene was used as an internal standard, and potentials were referenced to the ferrocene/ferrocenium couple.

4.3. PMMA film fabrication

A solution of PMMA (98 mg, 35 kDa) in dichloromethane (1.0 mL) was prepared at room temperature in a nitrogen-filled glovebox. Then, the respective iridium complex (2 mg, 2 wt %) was added to the solution and stirred until giving a homogeneous solution. The resulting solution was then drop-coated on a quartz substrate and dried at room temperature overnight.

4.4. X-ray crystallography details

Single crystals of **1f, 2a, 2b, 2c**, and **2d** were grown by layering CH_2Cl_2 or $CHCl_3$ solutions with hexane or diethyl ether. Crystals were mounted on a Bruker Apex II three-circle diffractometer using Mo$K\alpha$ radiation (λ = 0.71073 Å). The data were collected at 123(2) K and processed and refined within the APEXII software. Structures were solved by using intrinsic phasing in SHELXT and refined by standard difference Fourier techniques in the SHELXL program. All non-hydrogen atoms were refined with anisotropic displacement parameters. Hydrogen atoms bonded to carbon were fixed in calculated positions using the standard riding model and were refined isotropically. Hydrogen atoms bonded to nitrogen were located in the difference map and refined isotropically, restraining the N–H internuclear distance to 0.88 Å and the hydrogen displacement parameter to 1.2 × that of the nitrogen atom it is bonded to. In all structures except **2c**, disorder was observed in one or more locations of the main moiety, counterions, or solvent molecules. These include positional disorder of solvent molecules or alkyl groups and rotational disorders of PF_6^- counterions or CF_3 groups. All disordered parts were restrained with distance restraints (SADI in SHELX) and rigid-bond restraints (SIMU and DELU in SHELX). The crystal of **2c** was observed to be a non-merohedral twin and was refined against two unit cell domains. The twinning was not completely resolved, leading to some significant level A and level B checkCIF errors after refinement. As a result, the structural metrics (bond distances and bond lengths) in **2c** are not very reliable, but the final refined model does conclusively confirm the proposed molecular structure. Most of these high-level checkCIF errors originate from anomalously long or short refined bond distances, as well as one atom with a distorted ellipsoid and one solvent-accessible void space in the structure. In addition, the structure of **2d** returned one level B checkCIF error, originating from high residual electron density (3.24 electrons) near the disordered diethyl ether solvent molecule. Most of the electron density was satisfactorily modeled and the residual electron density did not have a significant impact on the refinement of the rest of the model. As such, we left the diethyl ether solvent as a two-part disorder in the final model and did not attempt to treat it as a more complex disorder or use the PLATON SQUEEZE function. All crystallographic details are summarized in Tables S1−S3.

4.5. Synthesis

4.5.1. Preparation of $[Ir(C^\wedge Y)_2(CNAr^{4\text{-}CF3})_2][PF_6]$ complexes 1c, 1e, and 1f

The Ir dimer $[Ir(C^\wedge Y)_2(\mu\text{-}Cl)]_2$ was dissolved in CH_2Cl_2 and combined with 2 equiv of $AgPF_6$. Then 4 equiv of 4-trifluoromethylphenyl isocyanide ($CNAr^{4\text{-}CF3}$) was added to the reaction mixture and stirred at room temperature overnight. The completed reaction mixture was filtered through Celite to remove AgCl. The filtrate volume was reduced, and diethyl ether was added to precipitate the product. The solid was dried under vacuum. The resulting crude product was purified by recrystallization from CH_2Cl_2/hexane or $CHCl_3$/diethyl ether to give a white solid.

4.5.1.1. $[Ir(pmi)_2(CNAr^{4\text{-}CF3})_2][PF_6]$ (1c). Prepared by the general procedure, using $[Ir(pmi)_2(\mu\text{-}Cl)]_2$ (1.0 g, 0.92 mmol). The product was crystallized from CH_2Cl_2/hexane to give a white solid (1.3 g, 71%). ^{1}H NMR (400 MHz, CD_3CN) δ: 7.81 (s, 2H, pmi*H*), 7.73 (d, J = 8.3 Hz, 4H, Ar*H*), 7.45 (d, J = 9.4 Hz, 6H, Ar*H*), 7.31 (d, J = 7.8 Hz, 2H, Ar*H*), 6.96 (t, J = 7.6 Hz, 2H, Ar*H*), 6.69 (t, J = 7.4 Hz, 2H, Ar*H*), 6.39 (d, J = 7.2 Hz, 2H, Ar*H*), 4.10 (s, 6H, NCH_3). ^{19}F NMR (376 MHz, CD_3CN) δ: −63.40 (s, 6F, CF_3), −72.73 (d, J = 706.5 Hz, 6F, PF_6).

4.5.1.2. $[Ir(ptrbz)_2(CNAr^{4\text{-}CF3})_2][PF_6]$ (1e). Prepared by the general procedure, using $[Ir(ptrbz)_2(\mu\text{-}Cl)]_2$ (1.0 g, 0.72 mmol). The product was crystallized from $CHCl_3$/diethyl ether to give a white solid (1.3 g, 79%). ^{1}H NMR (500 MHz, $CDCl_3$) δ: 7.89 (s, 2H, ptrbz*H*), 7.65 (d, J = 8.3 Hz, 4H, Ar*H*), 7.47 (m, 14H, Ar*H*), 7.36 (d, J = 7.5 Hz, 2H, Ar*H*), 6.90 (t, J = 7.5 Hz, 2H, Ar*H*), 6.79 (t, J = 7.5 Hz, 2H, Ar*H*), 6.06 (d, J = 7.5 Hz, 2H, Ar*H*), 5.77 (m, 4H, NCH_2Ar). ^{19}F NMR (470 MHz, $CDCl_3$) δ: −62.84 (s, 6F, CF_3), −72.64 (d, J = 712.8 Hz, 6F, PF_6). HRMS-ESI (*m/z*): $[M-PF_6]^+$ calcd for $C_{46}H_{32}F_{12}IrN_8$, 1003.2283; found, 1003.2287

4.5.1.3. $[Ir(F_2ptrbz)_2(CNAr^{4\text{-}CF3})_2][PF_6]$ (1f). Prepared by the general procedure, using $[Ir(F_2ptrbz)_2(\mu\text{-}Cl)]_2$ (1.0 g, 0.65 mmol). The product was crystallized from $CHCl_3$/diethyl ether to give a white solid (1.0 g, 63%). ^{1}H NMR (500 MHz, $CDCl_3$) δ: 7.92 (s, 2H, F_2ptrbz*H*), 7.69 (d, J = 8.4 Hz, 4H, Ar*H*), 7.62 (d, J = 8.3 Hz, 4H, Ar*H*), 7.47 (d, J = 10.7 Hz, 10H, Ar*H*), 6.47 (t, J = 8.8 Hz, 2H, F_2ptrbz*H*), 5.86 (m, 4H, NCH_2Ar), 5.57 (d, J = 8.0 Hz, 2H, F_2ptrbz*H*). ^{19}F NMR (470 MHz, $CDCl_3$) δ: −62.91 (s, 6F, CF_3), −72.64 (d, J = 712.7 Hz, 6F, PF_6), −107.48 (q, J = 8.4 Hz, Ar*F*), −110.41 (t, J = 8.9 Hz, Ar*F*). HRMS-ESI (*m/z*): $[M-PF_6]^+$ calcd for $C_{46}H_{28}F_{16}PIrN_8$, 1075.1907; found, 1075.1915

4.5.2. Preparation of $Ir(C^\wedge Y)_2(C_2H_3N_4(Ar^{4\text{-}CF3})_2)$ Complexes 2a-2f

Carbene complexes were synthesized following a procedure adapted from reported literature on related compounds[28,29]. The iridium bis-isocyanide complex $[Ir(C^\wedge Y)_2(CNAr^{4\text{-}CF3})_2][PF_6]$ (**1a**−**1f**) was dissolved in minimum CH_2Cl_2 then combined with excess hydrazine monohydrate and stirred at room temperature overnight. The completed reaction mixture was washed with deionized water. The aqueous layer was decanted and discarded, and the organic layer was dried with $MgSO_4$. The solution volume was reduced, and hexane or diethyl ether was added to induce precipitation. The solid was dried under vacuum. The resulting crude product was purified either by precipitation or recrystallization.

4.5.2.1. $Ir(F_2ptz)_2(C_2H_3N_4(Ar^{4\text{-}CF3})_2)$ (2a). Prepared by the general procedure, using $[Ir(F_2ptz)_2(CNAr^{4\text{-}CF3})_2][PF_6]$ (**1a**, 102 mg, 0.089 mmol) and $N_2H_4{\cdot}H_2O$ (1.0 mL, 21 mmol). The resulting product was precipitated from hexane to give a white powder. Yield: 87 mg, 92%. ^{1}H NMR (400 MHz, CD_3CN) δ: 10.24 (s, 1H, N*H*), 7.36 (d, J = 8.4 Hz, 4H, Ar*H*), 7.19 (d, J = 8.0 Hz, 4H, Ar*H*), 6.60–6.54 (m, 2H, Ar*H*), 6.41 (s, 2H, N*H*), 6.10 (dd, J = 8.0, 2.1 Hz, 2H, Ar*H*), 4.28 (s, 3H, NCH_3), 4.26 (s, 3H, NCH_3), 2.70–2.50 (m, 4H, CCH_2CH$_2$CH$_3$), 1.65 (td, J = 14.9, 7.5 Hz, 4H, CCH$_2$CH_2CH$_3$), 0.79 (t, J = 7.3 Hz, 6H, CCH$_2$CH$_2$CH_3). ^{19}F NMR (376 MHz, CD_2Cl_2) δ: −62.13 (s, 6F, ArCF_3), −102.94 (dd, J = 20.4, 8.2 Hz, 2F, Ar*F*), −107.81 (q, J = 8.7 Hz, 2F, Ar*F*). HRMS-ESI (*m/z*): $[M+H]^+$ calcd for $C_{40}H_{35}F_{10}IrN_{10}$, 1039.2594; found, 1039.2604.

4.5.2.2. Ir(CF$_3$ptz)$_2$(C$_2$H$_3$N$_4$(Ar$^{4\text{-CF3}}$)$_2$) (2b). Prepared by the general protocol, using [Ir(CF$_3$ptz)$_2$(CNAr$^{4\text{-CF3}}$)$_2$][PF$_6$] (**1b**, 50 mg, 0.041 mmol) and N$_2$H$_4$·H$_2$O (1.0 mL, 21 mmol). The product was purified by precipitation to form a yellow powder, which was dried in vacuo. Yield: 36 mg, 79%. ^{1}H NMR (400 MHz, CD$_3$CN) δ: 9.95 (s, 1H, N*H*), 7.85 (s, 2H, Ar*H*), 7.46 (d, J = 7.2 Hz, 4H, Ar*H*), 7.22 (d, J = 8.1 Hz, 4H, Ar*H*), 7.15 (d, J = 7.8 Hz, 2H, Ar*H*), 6.80 (d, J = 7.8 Hz, 2H, Ar*H*), 6.40 (s, 2H, N*H*), 4.25 (s, 6H, NC*H*$_3$), 2.71–2.52 (m, 4H, CC*H*$_2$CH$_2$CH$_3$), 1.66 (m, J = 14.7, 7.3 Hz, 4H, CCH$_2$C*H*$_2$CH$_3$), 0.80 (s, 6H, CCH$_2$CH$_2$C*H*$_3$). ^{19}F NMR (376 MHz, CD$_3$CN) δ: −62.14 (s, 12F, ArC*F*$_3$). HRMS-ESI (*m/z*): [M+H] $^+$ calcd for C$_{42}$H$_{37}$F$_{12}$IrN$_{10}$, 1103.2719; found, 1103.2721.

4.5.2.3. Ir(pmi)$_2$(C$_2$H$_3$N$_4$(Ar$^{4\text{-CF3}}$)$_2$) (2c). Prepared by the general protocol, using [Ir(pmi)$_2$(CNAr$^{4\text{-CF3}}$)$_2$] [PF$_6$] (**1c**, 100 mg, 0.10 mmol) and N$_2$H$_4$·H$_2$O (1.0 mL, 21 mmol). The product was purified by precipitation to form a white powder, which was dried in vacuo. Yield: 55 mg, 62%. ^{1}H NMR (600 MHz, CD$_2$Cl$_2$) δ: 9.87 (s, 1H, N*H*), 7.47 (d, J = 1.9 Hz, 2H, Ar*H*), 7.35 (d, J = 8.5 Hz, 4H, Ar*H*), 7.17 (d, J = 7.7 Hz, 2H, Ar*H*), 7.11 (d, J = 8.4 Hz, 4H, Ar*H*), 6.99 – 6.91 (m, 4H, Ar*H*), 6.78 (d, J = 6.1 Hz, 2H, Ar*H*), 6.74 (t, J = 7.0 Hz, 2H, Ar*H*), 6.58 (s, 2H, N*H*), 3.69 (s, 6H, NC*H*$_3$). ^{13}C{^{1}H} NMR (126 MHz, CD$_2$Cl$_2$) δ: 171.5, 148.71, 147.2, 143.7, 138.0, 126.3, 125.6, 123.4, 121.4, 121.3, 119.0, 114.7, 111.0, 36.8. ^{19}F NMR (565 MHz, CD$_2$Cl$_2$) δ: −62.03 (s, 6F, ArC*F*$_3$). HRMS-ESI (*m/z*): [M+H] $^+$ calcd for C$_{36}$H$_{29}$F$_6$IrN$_8$, 881.2123; found, 881.2106.

4.5.2.4. Ir(CF$_3$pmi)$_2$(C$_2$H$_3$N$_4$(Ar$^{4\text{-CF3}}$)$_2$) (2d). Prepared by the general protocol, using [Ir(CF$_3$pmi)$_2$(CNAr$^{4\text{-CF3}}$)$_2$][PF$_6$] (**1d**, 33 mg, 0.029 mmol) and N$_2$H$_4$·H$_2$O (1.0 mL, 21 mmol). The crude product was purified by precipitation from hexane to afford a light brown solid. Yield: 26 mg, 89%. ^{1}H NMR (600 MHz, CD$_2$Cl$_2$) δ: 9.65 (s, 1H, N*H*), 7.56 (s, 2H, Ar*H*), 7.46 (d, J = 7.6 Hz, 4H, Ar*H*), 7.39 (s, 2H, Ar*H*), 7.19 (d, J = 8.2 Hz, 4H, Ar*H*), 7.05 (s, 2H, Ar*H*), 6.99 (d, J = 6.9 Hz, 2H, Ar*H*), 6.91 (d, J = 7.6 Hz, 2H, Ar*H*), 6.40 (s, 2H, N*H*), 3.75 (s, 6H, NC*H*$_3$). ^{19}F NMR (565 MHz, CD$_2$Cl$_2$) δ: −61.77 (s, 6F, ArC*F*$_3$), −62.06 (s, 6F, ArC*F*$_3$). HRMS-ESI (*m/z*): [M+H] $^+$ calcd for C$_{38}$H$_{27}$F$_{12}$IrN$_8$, 1017.1875; found, 1017.1874.

4.5.2.5. Ir(ptrbz)$_2$(C$_2$H$_3$N$_4$(Ar$^{4\text{-CF3}}$)$_2$) (2e). Prepared by the general protocol, using [Ir(ptrbz)$_2$(CNAr$^{4\text{-CF3}}$)$_2$][PF$_6$] (**1e**, 145 mg, 0.13 mmol) and N$_2$H$_4$·H$_2$O (1.0 mL, 21 mmol). The crude product was purified by precipitation from hexane to afford a white solid. Yield: 101 mg, 77%. ^{1}H NMR (500 MHz, CD$_2$Cl$_2$) δ: 9.85 (s, 1H, N*H*), 7.59 (s, 2H, ptrbz*H*), 7.52 – 7.25 (m, 16H, Ar*H*), 7.19 (d, J = 8.3 Hz, 4H, Ar*H*), 6.88 (pent, J = 7.0 Hz, 4H, Ar*H*), 6.78 (s, 2H, N*H*), 6.55 (d, J = 6.9 Hz, 2H, Ar*H*), 5.62 (d, J = 14.8 Hz, 2H, NC*H*$_2$Ar), 5.47 (d, J = 14.8 Hz, 2H, NC*H*$_2$Ar). ^{13}C{^{1}H} NMR (126 MHz, CD$_2$Cl$_2$) δ: 166.7, 159.5, 136.3, 134.1, 132.2, 129.2, 129.1, 128.5, 128.4, 126.2, 121.8, 121.4, 117.7, 55.6. ^{19}F NMR (470 MHz, CD$_2$Cl$_2$) δ: −61.87 (s, 6F, ArC*F*$_3$). HRMS-ESI (*m/z*): [M+H]$^+$ calcd for C$_{46}$H$_{35}$F$_6$IrN$_{10}$, 1035.2658; found, 1035.2674

4.2.5.6. Ir(F$_2$ptrbz)$_2$(C$_2$H$_3$N$_4$(Ar$^{4\text{-CF3}}$)$_2$) (2f). Prepared by the general protocol, using [Ir(F$_2$ptrbz)$_2$(CNAr$^{4\text{-CF3}}$)$_2$][PF$_6$] (**1f**, 200 mg, 0.16 mmol) and N$_2$H$_4$·H$_2$O (1.0 mL, 21 mmol). The crude product was purified by precipitation from hexane to afford a light yellow solid. Yield: 98 mg, 56%. ^{1}H NMR (600 MHz, CD$_2$Cl$_2$) δ: 9.84 (s, 1H, N*H*), 7.72 (s, 2H, F$_2$ptrbz*H*), 7.50 – 7.30 (m, 15H, Ar*H*), 7.24 (d, J = 8.3 Hz, 4H, Ar*H*), 6.65 (s, 2H, N*H*), 6.43 (t, J = 10.7 Hz, 2H, F$_2$ptrbz*H*), 6.01 (d, J = 10.1 Hz, 2H, F$_2$ptrbz*H*), 5.66 (d, J = 14.8 Hz, 2H, NC*H*$_2$Ar), 5.53 (d, J = 14.8 Hz, 2H, NC*H*$_2$Ar). ^{19}F NMR (565 MHz, CD$_2$Cl$_2$) δ: −61.99 (s, 6F, ArC*F*$_3$), −110.73 (s, 2F, *F*$_2$ptrbz), −113.30 (s, 2F, *F*$_2$ptrbz). HRMS-ESI (*m/z*): [M+H] $^+$ calcd for C$_{46}$H$_{31}$F$_{10}$IrN$_{10}$, 1107.2278; found, 1107.2275.

Declaration of Competing Interest

The authors declare that they have no known competing financial interests or personal relationships that could have appeared to influence the work reported in this paper

Data availability

Data will be made available on request.

Acknowledgment

We acknowledge the Welch Foundation (Grant E-1887) and the National Science Foundation (Grant CHE-1846831) for funding this work.

Supplementary materials

Supplementary material associated with this article can be found, in the online version, at doi:10.1016/j.jorganchem.2022.122561.

References

[1] Y. Wu, G.D. Sutton, M.D.S. Halamicek, X. Xing, J. Bao, T.S. Teets, Cyclometalated iridium-coumarin ratiometric oxygen sensors: improved signal resolution and tunable dynamic ranges, Chem. Sci. (2022), doi:10.1039/D2SC02909J.
[2] J.S. Nam, M.-G. Kang, J. Kang, S.-Y. Park, S.J.C. Lee, H.-T. Kim, J.K. Seo, O.-H. Kwon, M.H. Lim, H.-W. Rhee, T.-H. Kwon, Endoplasmic reticulum-localized iridium(III) complexes as efficient photodynamic therapy agents via protein modifications, J. Am. Chem. Soc. 138 (2016) 10968–10977, doi:10.1021/jacs.6b05302.
[3] J.-H. Shon, D. Kim, M.D. Rathnayake, S. Sittel, J. Weaver, T.S. Teets, Photoredox catalysis on unactivated substrates with strongly reducing iridium photosensitizers, Chem. Sci. 12 (2021) 4069–4078, doi:10.1039/D0SC06306A.
[4] P.-Y. Ho, C.-L. Ho, W.-Y. Wong, Recent advances of iridium(III) metallophosphors for health-related applications, Coord. Chem. Rev. 413 (2020) 213267, doi:10.1016/j.ccr.2020.213267.
[5] J. Lee, H.-F. Chen, T. Batagoda, C. Coburn, P.I. Djurovich, M.E. Thompson, S.R. Forrest, Deep blue phosphorescent organic light-emitting diodes with very high brightness and efficiency, Nat. Mater. 15 (2016) 92–98, doi:10.1038/nmat4446.
[6] A.K. Pal, S. Krotkus, M. Fontani, C.F.R. Mackenzie, D.B. Cordes, A.M.Z. Slawin, I.D.W. Samuel, E. Zysman-Colman, High-efficiency deep-blue-emitting organic light-emitting diodes based on iridium(III) carbene complexes, Adv. Mater. 30 (2018) 1804231, doi:10.1002/adma.201804231.
[7] H. Sasabe, J. Takamatsu, T. Motoyama, S. Watanabe, G. Wagenblast, N. Langer, O. Molt, E. Fuchs, C. Lennartz, J. Kido, High-efficiency blue and white organic light-emitting devices incorporating a blue iridium carbene complex, Adv. Mater. 22 (2010) 5003–5007, doi:10.1002/adma.201002254.
[8] P.-N. Lai, C.H. Brysacz, M.K. Alam, N.A. Ayoub, T.G. Gray, J. Bao, T.S. Teets, Highly efficient red-emitting bis-cyclometalated iridium complexes, J. Am. Chem. Soc. 140 (2018) 10198–10207, doi:10.1021/jacs.8b04841.
[9] P.-T. Chou, Y. Chi, Phosphorescent dyes for organic light-emitting diodes, Chem. Eur. J. 13 (2007) 380–395, doi:10.1002/chem.200601272.
[10] A.F. Rausch, H.H.H. Homeier, H. Yersin, Organometallic Pt(II) and Ir(III) triplet emitters for OLED applications and the role of spin–orbit coupling: a study based on high-resolution optical spectroscopy, in: A.J. Lees (Ed.), Photophysics Organomet, Springer, Berlin, Heidelberg, 2010, pp. 193–235, doi:10.1007/3418_2009_6.
[11] Organic Light-Emitting Diodes (OLEDs). 1st Ed., (n.d.). https://www.elsevier.com/books/organic-light-emitting-diodes-oleds/buckley/978-0-85709-425-4 (accessed August 2, 2022).
[12] T. Sajoto, P.I. Djurovich, A. Tamayo, M. Yousufuddin, R. Bau, M.E. Thompson, R.J. Holmes, S.R. Forrest, Blue and near-UV phosphorescence from iridium complexes with cyclometalated pyrazolyl or N-heterocyclic carbene ligands, Inorg. Chem. 44 (2005) 7992–8003, doi:10.1021/ic051296i.
[13] K.-Y. Lu, H.-H. Chou, C.-H. Hsieh, Y.-H.O. Yang, H.-R. Tsai, H.-Y. Tsai, L.-C. Hsu, C.-Y. Chen, I.-C. Chen, C.-H. Cheng, Wide-range color tuning of iridium bis-carbene complexes from blue to red by different N^N ligands: an alternative route for adjusting the emission colors, Adv. Mater. 23 (2011) 4933–4937, doi:10.1002/adma.201102886.
[14] Z. Chen, L. Wang, C.-L. Ho, S. Chen, S. Suramitr, A. Plucksacholatarn, N. Zhu, S. Hannongbua, W.-Y. Wong, Smart design on the cyclometalated ligands of iridium(III) complexes for facile tuning of phosphorescence color spanning from deep-blue to near-infrared, Adv. Opt. Mater. 6 (2018) 1800824, doi:10.1002/adom.201800824.

[15] Z. Chen, L. Wang, S. Su, X. Zheng, N. Zhu, C.-L. Ho, S. Chen, W.-Y. Wong, Cyclometalated iridium(III) carbene phosphors for highly efficient blue organic light-emitting diodes, ACS Appl. Mater. Interfaces. 9 (2017) 40497–40502, doi:10.1021/acsami.7b09172.
[16] X. Li, J. Zhang, Z. Zhao, L. Wang, H. Yang, Q. Chang, N. Jiang, Z. Liu, Z. Bian, W. Liu, Z. Lu, C. Huang, Deep blue phosphorescent organic light-emitting diodes with CIEy value of 0.11 and external quantum efficiency up to 22.5%, Adv. Mater. 30 (2018) 1705005, doi:10.1002/adma.201705005.
[17] T.-Y. Li, X. Liang, L. Zhou, C. Wu, S. Zhang, X. Liu, G.-Z. Lu, L.-S. Xue, Y.-X. Zheng, J.-L. Zuo, N-heterocyclic carbenes: versatile second cyclometalated ligands for neutral iridium(III) heteroleptic complexes, Inorg. Chem. 54 (2015) 161–173, doi:10.1021/ic501949h.
[18] X. Liang, F. Zhang, Z.-P. Yan, Z.-G. Wu, Y. Zheng, G. Cheng, Y. Wang, J.-L. Zuo, Y. Pan, C.-M. Che, Fast synthesis of iridium(III) complexes incorporating a bis(diphenylphorothioyl)amide ligand for efficient pure green OLEDs, ACS Appl. Mater. Interfaces. 11 (2019) 7184–7191, doi:10.1021/acsami.8b19318.
[19] H. Na, L.M. Cañada, Z. Wen, J.I.-C. Wu, T.S. Teets, Mixed-carbene cyclometalated iridium complexes with saturated blue luminescence, Chem. Sci. 10 (2019) 6254–6260, doi:10.1039/C9SC01386E.
[20] L.M. Cañada, J. Kölling, Z. Wen, J.I.-C. Wu, T.S. Teets, Cyano-isocyanide iridium(III) complexes with pure blue phosphorescence, Inorg. Chem. 60 (2021) 6391–6402, doi:10.1021/acs.inorgchem.1c00103.
[21] S. Haneder, E. Da Como, J. Feldmann, J.M. Lupton, C. Lennartz, P. Erk, E. Fuchs, O. Molt, I. Münster, C. Schildknecht, G. Wagenblast, Controlling the radiative rate of deep-blue electrophosphorescent organometallic complexes by singlet-triplet gap engineering, Adv. Mater. 20 (2008) 3325–3330, doi:10.1002/adma.200800630.
[22] J.M. Fernández-Hernández, J.I. Beltrán, V. Lemaur, M.-D. Gálvez-López, C.-H. Chien, F. Polo, E. Orselli, R. Fröhlich, J. Cornil, L. De Cola, Iridium(III) emitters based on 1,4-disubstituted-1*H*-1,2,3-triazoles as cyclometalating ligand: synthesis, characterization, and electroluminescent devices, Inorg. Chem. 52 (2013) 1812–1824, doi:10.1021/ic3018419.
[23] Y. You, S.Y. Park, Inter-ligand energy transfer and related emission change in the cyclometalated heteroleptic iridium complex: facile and efficient color tuning over the whole visible range by the ancillary ligand structure, J. Am. Chem. Soc. 127 (2005) 12438–12439, doi:10.1021/ja052880t.
[24] L. Tschugajeff, M. Skanawy-Grigorjewa, Reaction of K_2PtCl_4 with isonitriles and hydrazine, J. Russ. Chem. Soc. 47 (1915) 776.
[25] L. Tschugajeff, M. Skanawy-Grigorjewa, A. Posnjak, Über die hydrazincarbylamin-komplexe des platins, Z. Für Anorg. Allg. Chem. 148 (1925) 37–42, doi:10.1002/zaac.19251480105.
[26] W.M. Butler, J.H. Enemark, J. Parks, A.L. Balch, Chelative addition of hydrazines to coordinated isocyanides. Structure of Chugaev's red salt, Inorg. Chem. 12 (1973) 451–457, doi:10.1021/ic50120a042.
[27] L.M. Slaughter, Acyclic aminocarbenes in catalysis, ACS Catal 2 (2012) 1802–1816, doi:10.1021/cs300300y.
[28] H. Na, A. Maity, R. Morshed, T.S. Teets, Bis-cyclometalated iridium complexes with chelating dicarbene ancillary ligands, Organometallics 36 (2017) 2965–2972, doi:10.1021/acs.organomet.7b00428.
[29] H. Na, P. Lai, L.M. Cañada, T.S. Teets, Photoluminescence of cyclometalated iridium complexes in poly(methyl methacrylate) films, Organometallics 37 (2018) 3269–3277, doi:10.1021/acs.organomet.8b00446.
[30] Y. Wu, Z. Wen, J.I. Wu, T.S. Teets, Efficient deep blue platinum acetylide phosphors with acyclic diaminocarbene ligands, Chem. Eur. J. 26 (2020) 16028–16035, doi:10.1002/chem.202002775.
[31] Y.H. Nguyen, J.V. Soares, S.H. Nguyen, Y. Wu, J.I. Wu, T.S. Teets, Platinum(II)-substituted phenylacetylide complexes supported by acyclic diaminocarbene ligands, Inorg. Chem. 61 (2022) 8498–8508, doi:10.1021/acs.inorgchem.2c00510.
[32] H. Na, T.S. Teets, Highly luminescent cyclometalated iridium complexes generated by nucleophilic addition to coordinated isocyanides, J. Am. Chem. Soc. 140 (2018) 6353–6360, doi:10.1021/jacs.8b02416.
[33] L.M. Cañada, J. Kölling, T.S. Teets, Blue-phosphorescent bis-cyclometalated iridium complexes with aryl isocyanide ancillary ligands, Polyhedron 178 (2020) 114332, doi:10.1016/j.poly.2019.114332.
[34] C. Jiang, T.S. Teets, Trimetallic iridium–nickel–iridium bis(formazanate) assemblies, Inorg. Chem. 61 (2022) 8788–8796, doi:10.1021/acs.inorgchem.2c00726.
[35] P. Lai, S. Yoon, Y. Wu, T.S. Teets, Effects of ancillary ligands on deep red to near-infrared cyclometalated iridium complexes, ACS Org. Inorg. Au. 2 (2022) 236–244, doi:10.1021/acsorginorgau.1c00044.
[36] A. Baschieri, L. Sambri, A. Mazzanti, A. Carlone, F. Monti, N. Armaroli, Iridium(III) complexes with fluorinated phenyl-tetrazoles as cyclometalating ligands: enhanced excited-state energy and blue emission, Inorg. Chem. 59 (2020) 16238–16250, doi:10.1021/acs.inorgchem.0c01995.
[37] M. Nonoyama, Benzo[*h*]quinolin-10-yl-N iridium(III) complexes, Bull. Chem. Soc. Jpn. 47 (1974) 767–768, doi:10.1246/bcsj.47.767.